Electron spin dynamics in cubic GaN

J. H. Buß,[1] T. Schupp,[2] D. J. As,[2] O. Brandt,[3] D. Hägele,[1] and J. Rudolph[1]

[1]*Arbeitsgruppe Spektroskopie der kondensierten Materie, Ruhr-Universität Bochum, Universitätsstraße 150, D-44780 Bochum, Germany*
[2]*Department of Physics, University of Paderborn, Warburger Str. 100, D-33095 Paderborn, Germany*
[3]*Paul-Drude-Institut für Festkörperelektronik, Hausvogteiplatz 5-7, 10117 Berlin, Germany*

The electron spin dynamics in cubic GaN is comprehensively investigated by time-resolved magneto-optical Kerr-rotation spectroscopy over a wide range of temperatures, magnetic fields, and doping densities. The spin dynamics is found to be governed by the interplay of spin relaxation of localized electrons and Dyakonov-Perel relaxation of delocalized electrons. Localized electrons significantly contribute to spin relaxation up to room temperature at moderate doping levels, while Dyakonov-Perel relaxation dominates for high temperatures or degenerate doping levels. Quantitative agreement to Dyakonov-Perel theory requires a larger value of the spin-splitting constant than theoretically predicted. Possible reasons for this discrepancy are discussed, including the role of charged dislocations.

I. INTRODUCTION

Spin relaxation of conduction band electrons is generally governed by Dyakonov-Perel (DP) spin relaxation in the majority of *n*-type III-V semiconductors [1,2]. DP relaxation is based on an intrinsic spin splitting of the conduction band caused by spin-orbit coupling (SOC) [3], whose strength increases as a rule of thumb with the atomic number of the constituent group-III and group-V elements [4,5]. Consequently, weaker SOC and hence weaker DP relaxation are expected for GaN in comparison to, e.g., GaAs. GaN has therefore been considered as a promising material system for spintronics, where long spin-relaxation times are a prerequisite for possible applications [6–9]. SOC is, however, also strongly dependent on the symmetry of the semiconductor crystal lattice, and DP relaxation was shown to be very efficient in the thermodynamically favored wurtzite crystal phase of GaN (α-GaN) due to its lower symmetry as compared to cubic semiconductors [10–15]. This intrinsic limitation of spin coherence was predicted to be lifted in the metastable zincblende phase of GaN (β-GaN) [16,17], and long spin-relaxation times were indeed experimentally demonstrated at high temperatures and high doping levels in cubic GaN [18,19]. The experimentally found spin-relaxation times were, however, still substantially shorter than predicted by DP theory. The systematic investigation of electron spin relaxation in cubic GaN is therefore of high interest not only for possible applications in spintronics but also for fundamental aspects of spin relaxation in semiconductors. The study of spin relaxation in semiconductor systems with presumably weak DP relaxation potentially allows the observation of otherwise hidden spin-relaxation mechanisms, like in the case of intersubband relaxation in GaAs(110) quantum wells [20].

Here, we systematically investigate electron spin relaxation in cubic GaN by time-resolved Kerr-rotation (TRKR) spectroscopy over a wide range of temperatures, external magnetic fields, and doping densities. We find a complex interplay of spin relaxation of localized electrons and Dyakonov-Perel relaxation of delocalized electrons, with localized electrons governing the spin relaxation up to moderate temperature and doping densities. Dyakonov-Perel spin relaxation dominates in the regime of high temperatures and high doping densities. Quantitative agreement to Dyakonov-Perel is obtained for significantly larger values of the spin-splitting constant than theoretically predicted.

The paper is organized as follows. In Sec. II, we first review the theoretical basis of spin relaxation in semiconductors. The experimental technique and the investigated samples are presented in Sec. III, followed by the experimental results and their discussion in Sec. IV.

II. THEORY

Electron spin relaxation in semiconductors is generally driven by several physically distinct mechanisms. The strength of these different mechanisms depends on numerous parameters like the band structure of the semiconductor as an intrinsic property, but also on extrinsic parameters like temperature or magnetic field. In the following, we will briefly discuss mechanisms that are important for electron spin relaxation in cubic GaN. First, we address the theory of DP spin relaxation for free, delocalized electrons, before we turn to the case of spin relaxation of strongly localized electrons. Finally, we briefly review spin relaxation due to the Elliott-Yafet mechanism and the Bir-Aronov-Pikus mechanism, which are only of minor importance for spin relaxation in β-GaN.

A. Dyakonov-Perel spin relaxation

Dyakonov-Perel spin relaxation of delocalized electrons is driven by a spin splitting of the conduction band in combination with momentum scattering. The SOC induced spin splitting acts as a wave-vector-dependent effective magnetic field $\mathbf{\Omega}(\mathbf{k})$ on the electrons' spins, which consequently precess around the effective magnetic field axis. Momentum scattering leads to random changes of the wave vector, resulting in a fluctuating effective magnetic field, which finally causes spin dephasing for an ensemble of electrons. The conduction band spin splitting is given by the Hamiltonian

$$H_{\text{soc}} = \frac{\hbar}{2}\mathbf{\Omega}(\mathbf{k}) \cdot \boldsymbol{\sigma} \tag{1}$$

with σ as the vector of Pauli spin matrices. The formal correspondence of H_{soc} to the Zeeman Hamiltonian for electrons in an external magnetic field readily illustrates the interpretation of $\boldsymbol{\Omega}(\mathbf{k})$ as an effective magnetic field. Generally, different effects contribute to the conduction band spin splitting, leading to a total effective magnetic field

$$\boldsymbol{\Omega}_{\text{total}}(\mathbf{k}) = \sum_i \boldsymbol{\Omega}_i(\mathbf{k}) . \tag{2}$$

An intrinsic contribution to the conduction band spin splitting in bulk semiconductors with zinc-blende structure stems from the Dresselhaus term [21]

$$\boldsymbol{\Omega}_D(\mathbf{k}) = \frac{2\gamma_e}{\hbar} \begin{pmatrix} k_x(k_y^2 - k_z^2) \\ k_y(k_z^2 - k_x^2) \\ k_z(k_x^2 - k_y^2) \end{pmatrix} \tag{3}$$

with the material specific spin-splitting constant γ_e. Further contributions to $\boldsymbol{\Omega}_{\text{total}}(\mathbf{k})$ can arise, e.g., from strain-induced spin splittings [22,23].

In the most basic approach to DP theory, the individual efficiencies and energy dependencies of different momentum scattering mechanisms are neglected and the tensor $\gamma_{s,ij}^{\text{simp}}$ of the spin-relaxation rates is given by [24]

$$\gamma_{s,ij}^{\text{simp}} = \tfrac{1}{2}(\delta_{ij}\langle\overline{\boldsymbol{\Omega}^2}\rangle - \langle\overline{\Omega_i\Omega_j}\rangle)\tau_p, \tag{4}$$

where $\overline{\ldots}$ and $\langle\ldots\rangle$ denote the average over the angular momentum distribution and the energy distribution of the electrons, respectively, and τ_p is an effective, averaged momentum scattering time.

A more accurate description of DP relaxation by Pikus and Titkov [25] accounts for the different efficiencies and energy dependencies of momentum scattering mechanisms by including efficiency factors γ_ℓ in the expression for the tensor $\tilde{\gamma}_{s,ij}$ of energy dependent spin-relaxation rates,

$$\tilde{\gamma}_{s,ij} = (\delta_{ij}\overline{\boldsymbol{\Omega}^2} - \overline{\Omega_i\Omega_j})\left(\sum_\nu \frac{\gamma_{\ell,\nu}}{\tilde{\tau}_{p,\nu}}\right)^{-1}, \quad i,j = x,y,z , \tag{5}$$

where $\tilde{\tau}_{p,\nu}$ is the energy dependent momentum scattering time and $\gamma_{\ell,\nu}$ the efficiency factor of the νth momentum scattering mechanism. The Hamiltonian $H_{soc} \propto k^\ell$ is polynomial in the magnitude of the wave vector, with the k^3-dependent Dresselhaus term corresponding to $\ell = 3$, while contributions linear in k, such as strain-induced spin splittings, correspond to $\ell = 1$ with $\gamma_1 = 1$ [1,8,26]. Considering only the Dresselhaus term, the directional average readily gives the isotropic spin-relaxation rate

$$\tilde{\gamma}_{s,ij} = \delta_{ij}\frac{32}{105}\frac{\gamma_e^2}{\hbar^2}k^6\left(\sum_\nu \frac{\gamma_{\ell,\nu}}{\tilde{\tau}_{p,\nu}}\right)^{-1}. \tag{6}$$

The energy average is carried out for nondegenerate electrons by assuming a Boltzmann distribution for the electron momentum distribution, leading to, approximately

$$\gamma_s^{\text{DP,nd}} = \langle\Omega_{\text{eff,nd}}^2\rangle(Q\tau_p)_{\text{total}} \tag{7}$$

with

$$\langle\Omega_{\text{eff,nd}}^2\rangle \equiv \frac{8m^{*3}(k_BT)^3}{\hbar^8}\gamma_e^2 \tag{8}$$

TABLE I. Values of the efficiency factors γ_3 and efficiency coefficients Q for different momentum scattering mechanisms.

Scattering mechanism	γ_3	Q	Reference
polar optical phonon	11/6	1152/385	[18,25,27]
ionized impurity	6	32/21	[25]
deformation potential	1	96/35	[25]
piezoelectric	11/6	1152/385	[25]
dislocation	6	32/21	[18,28]

and

$$(Q\tau_p)_{\text{total}} \equiv \left(\sum_\nu 1/(\tau_{p,\nu}Q_\nu)\right)^{-1}, \tag{9}$$

where $\tau_{p,\nu} = \langle\tilde{\tau}_{p,\nu}E_k\rangle/\langle E_k\rangle$. The efficiency coefficients Q_ν depend on the specific momentum scattering mechanism and are given by

$$Q_\nu = \frac{32}{105}\frac{1}{\gamma_{\ell,\nu}}\frac{\langle\tilde{\tau}_{p,\nu}E_k^3\rangle\langle E_k\rangle}{\langle\tilde{\tau}_{p,\nu}E_k\rangle(k_BT)^3} . \tag{10}$$

Assuming a power-law dependence $\tilde{\tau}_{p,\nu} \propto E_k^n$ for the energy dependence of the momentum scattering time, the efficiency coefficients can be expressed as

$$Q_\nu = \frac{16}{35}\frac{1}{\gamma_{\ell,\nu}}\left(n + \frac{7}{2}\right)\left(n + \frac{5}{2}\right). \tag{11}$$

The corresponding values of the efficiency factors γ_ℓ and efficiency coefficients Q_ν for different momentum scattering mechanisms are given in Table I.

In the degenerate regime, the absolute value k of the electron wave vector is replaced by the Fermi wave vector $k_F = (3\pi^2)^{1/3}n_D^{1/3}$ in Eq. (6) as only electrons at the Fermi edge contribute significantly to scattering. The spin-relaxation rate

$$\gamma_s^{\text{DP,deg}} = \langle\Omega_{\text{eff,deg}}^2\rangle\tau_{p,\text{eff}}^{\text{deg}} \tag{12}$$

follows accordingly for the degenerate regime, where n_D is the electron density,

$$\langle\Omega_{\text{eff,deg}}^2\rangle \equiv \frac{96\pi^4\gamma_e^2}{35\hbar^2}n_D^2 , \tag{13}$$

and

$$\tau_{p,\text{eff}}^{\text{deg}} \equiv \left(\sum_\nu \frac{\gamma_{\ell,\nu}}{\tau_{p,\nu}(E_F)}\right)^{-1} \tag{14}$$

is the effective momentum scattering time.

In the presence of an external magnetic field, DP spin relaxation is additionally influenced by spin Larmor precession and orbital cyclotron motion, respectively [29]. Larmor precession around the external magnetic field can efficiently suppress the precession around the fluctuating internal effective magnetic field [30], thus leading to a slowdown of DP relaxation according to [1,25]

$$\gamma_s^{\text{DP}}(B_{\text{ext}}) = \frac{\gamma_{s,0}^{\text{DP}}}{1 + (\omega_L\tau_p)^2} \tag{15}$$

with the Larmor precession frequency $\omega_L = g \mu_B B_{ext}/\hbar$, the Landé g factor, the spin-relaxation rate at zero magnetic field $\gamma_{s,0}^{DP}$, and the effective, averaged momentum scattering time τ_p. A slowdown of DP relaxation results also from the orbital motion of electrons in a nonquantizing external magnetic field, which leads to a cyclotron motion of the electrons. The longitudinal component of the electronic quasimomentum is conserved in this case, while the transversal components precess with the cyclotron frequency $\omega_c = q B_{ext}/m^*$. The resulting averaging of the fluctuating effective magnetic field leads to suppression of DP relaxation according to [1,31]

$$\gamma_s^{DP}(B_{ext}) \approx \frac{\gamma_{s,0}^{DP}}{1 + (\omega_c \tau_p)^2} \ . \tag{16}$$

B. Spin relaxation of localized electrons

Electrons strongly localized at defects have zero average wave vectors, hence the DP spin-relaxation mechanism discussed in the previous section is efficiently suppressed. Instead, the spin relaxation of localized electrons is driven by hyperfine interaction with the nuclei of lattice atoms or by spin-orbit interactions [34]. In the former case, localized electrons interact via hyperfine Fermi contact interaction with the large number of nuclei in the localization volume of the electron. This hyperfine interaction corresponds to an effective nuclear magnetic field, which acts on the electron spin and whose fluctuations cause dephasing of the electron spin. The spin dephasing time due to the fluctuating hyperfine field follows for completely isolated electrons as [1,35,36]

$$\gamma_s^{HF} = \frac{1}{\hbar} \sqrt{\frac{2 \sum_j I_j(I_j+1) A_j^2 y_j}{3 N_L}} \ , \tag{17}$$

where the sum runs over the nuclear isotopes with y_j as the abundance, A_j as the hyperfine constant and I_j as the nuclear spin of isotope j. The number N_L of nuclei that effectively interact with the electron is estimated via the ratio of the electron localization volume V_L to the volume v_0 of the unit cell. The electron localization volume V_L may further be approximated by the volume $V_e = 4/3\pi a_e^3$ with a modified Bohr radius $a_e = 1.5\varepsilon/(m^*/m_e)a_H$, where ε is the static dielectric constant and a_H the Bohr radius of an H atom [37].

For increasing donor density n_D, electron hopping between donors limits the correlation time τ_c of spin precession in the fluctuating nuclear field. The spin dephasing rate is then given by [30,34]

$$\gamma_s^{HF,h} = \frac{2}{3} \langle \omega_{nucl}^2 \rangle \tau_c \tag{18}$$

with $\langle \omega_{nucl}^2 \rangle = (v_0/8\pi \hbar^2 a_e^3) \sum_j I_j(I_j+1) A_j^2$ being the mean square of the spin precession frequency in the fluctuating nuclear field.

Spin relaxation of localized electrons can also be driven by spin-orbit interaction, which results in an anisotropic contribution to the exchange interaction between localized electrons [38]. Qualitatively, spin-orbit interaction leads to small rotations of the electron spins if two localized electrons exchange positions. These spin rotations can be ascribed to a corresponding fluctuating effective magnetic field, which

finally leads to spin dephasing. The spin dephasing rate due to this anisotropic exchange interaction follows as [39]

$$\gamma_s^{aex} = \frac{2}{3} \langle \varphi^2 \rangle \tau_c^{-1} \ , \tag{19}$$

where $\langle \varphi^2 \rangle$ is the mean-squared value of the angle φ of spin rotation due to the exchange.

For localized electrons, an external magnetic field leads generally to a linear increase of the spin-relaxation rate

$$\gamma_s^{HF} \propto B_{ext} \tag{20}$$

for high magnetic fields B_{ext} [13,36,37,40], which might be explained by variations Δg of the g factor, leading to inhomogeneous dephasing.

C. Other spin-relaxation mechanisms

Generally, spin relaxation in semiconductors can be caused by several other mechanisms than the ones discussed in the previous sections. In the following, we will give a brief overview of these mechanisms.

Spin relaxation of delocalized electrons due to the so-called Elliott-Yafet (EY) mechanism is based on the mixing of spin-up and spin-down electron states by spin-orbit coupling [1,8,41,42]. Due to this mixing, spin-independent momentum scattering can cause spin flips, resulting finally in spin relaxation. The spin-relaxation rate due to the Elliott-Yafet mechanism can be estimated by the relation for the long-range interaction part, which is usually dominating in III-V semiconductors [1,43],

$$\gamma_s^{EY} = A \left(\frac{E}{E_g} \right)^2 \eta^2 \left(\frac{1-\eta/2}{1-\eta/3} \right)^2 \frac{1}{\tau_p}, \tag{21}$$

where $E = k_B T$ in the nondegenerate regime and $E = E_F$ in the degenerate regime, respectively, $\eta = \Delta_{so}/(E_g + \Delta_{so})$ with E_g as the band-gap energy and Δ_{so} as the spin-orbit splitting, and A is a dimensionless constant between 2 and 6 depending on the dominating momentum scattering mechanism.

Electron scattering with holes can lead to electron spin relaxation via simultaneous spin flips due to the electron-hole exchange interaction. The effectiveness of this so-called Bir-Aronov-Pikus (BAP) mechanism depends strongly on the state of the holes, resulting in a complex dependence of spin relaxation on hole density and temperature [44]. Several approximate expressions have been derived for limiting cases such as scattering of electrons by holes bound to acceptors or by free, nondegenerate holes [1,25]. Generally, the BAP mechanism is, however, only relevant for substantial hole concentrations [2].

The wave-vector or energy dependence of the Landé g factor can additionally lead to spin relaxation, which speeds up for increasing external magnetic field [45]. This mechanism becomes, however, important only for high magnetic fields [46].

D. Total spin-relaxation rate

In general, both localized and free, delocalized electrons exist in the semiconductor. Efficient exchange scattering leads, however, to spin-relaxation times common for both systems [34,47,48]. The corresponding spin-relaxation rate

TABLE II. Values of the Dresselhaus spin-splitting constant γ_e from different theoretical models.

γ_e (eVÅ^3)	Model	Reference
0.508	sp^3s^* tight-binding	Refs. [32,33]
0.235	$sp^3d^5s^*$ tight-binding	Ref. [33]
0.84	tight-binding, empirical pseudopotential	Ref. [19]

observed in the experiment follows approximately as [48]

$$\gamma_s \approx \frac{n_{\text{loc}}/n_{\text{total}}}{\tau_s^{\text{loc}}} + \frac{n_{\text{deloc}}/n_{\text{total}}}{\tau_s^{\text{deloc}}}, \qquad (22)$$

where n_{total} is the total electron density, and n_{loc} and n_{deloc} are the densities of localized and delocalized electrons, respectively, with τ_s^{loc} and τ_s^{deloc} as the corresponding spin-relaxation times for localized and delocalized electrons, respectively.

III. SAMPLES AND EXPERIMENTAL SETUP

All β-GaN samples under investigation were grown by plasma-assisted molecular beam epitaxy (MBE) [49–51]. Table III summarizes details on the layer structure of the investigated samples, which fall in four groups: samples belonging to group A were grown on top of a β-AlN buffer layer [52] on 3C-SiC/Si(001) substrates, with Si doping of the top β-GaN layer resulting in n-type doping densities [53] n_D from $n_D = 1 \times 10^{17}$ cm^{-3} up to 1.5×10^{19} cm^{-3}. The phase purity of the β-GaN layer was verified by high resolution x-ray diffraction (HRXRD) measurements (see Table IV). The β-GaN epilayers for the samples of group B were directly grown on 3C-SiC/Si(001) substrates and exhibit n-type doping densities from $n_D = 1 \times 10^{17}$ cm^{-3} up to 1×10^{18} cm^{-3}. Sample C consists of 400 nm β-GaN grown on a 30 nm-thick SiC layer produced by carbonizing a Si(001) substrate [54], resulting in a low residual electron doping density of $n_D = 6 \times 10^{16}$ cm^{-3} of the β-GaN layer. Sample D was grown on a GaAs(001) substrate, and exhibits a background electron doping density of $n_D = 8 \times 10^{17}$ cm^{-3} with a mobility of 75 cm^2/Vs as determined by Hall measurements [51].

Time-resolved photoluminescence (PL) measurements were performed with the frequency-doubled output of a

TABLE IV. Phase purity of samples A2-A7 as determined by high resolution x-ray diffraction.

sample	phase purity (%)
A2	99.5
A3	99.8
A4	99.3
A5	99.7
A6	97.5
A7	99.7

femtosecond-mode-locked Ti:sapphire laser with a repetition rate of 80 MHz for excitation, and a synchroscan streak-camera system for energy- and time-resolved detection. The excitation energy was fixed at 3.55 eV and an average excitation power of 8 mW was used.

For the TRKR measurements, the output of a femtosecond-mode-locked Ti:sapphire-laser was frequency-doubled and split into pump and probe beam. The pump beam was polarization-modulated between right and left circularly polarized, respectively, at a frequency of 50 kHz by a photoelastic modulator, before it was focused down to a spot with a diameter of approximately 100 μm on the sample surface. The temporal evolution of the spin-polarization of the electron ensemble initially created by the pump pulses was tracked via the Kerr rotation of the linearly polarized probe pulses, which were temporally delayed via a variable mechanical delay line. A cascaded lock-in amplifier detection scheme using the fast polarization modulation of the pump pulses and a significantly slower amplitude modulation of the probe pulses was employed for a good signal-to-noise ratio. The energy of pump and probe was set to the maximum of the TRKR signal, corresponding to 3.280 eV for the lowest doped samples and 3.293 eV for the samples with the highest doping level, respectively, at low temperatures. For increasing temperature, these energies redshifted following the temperature-induced decrease of the band gap. The average pump and probe power was 10 and 1 mW, respectively. The samples were mounted in a cold-finger cryostat and an external magnetic field B_{ext} was applied in the sample plane.

TABLE III. Doping density, layer structure, and substrate of samples A1-A7, B1-B3, C, and D.

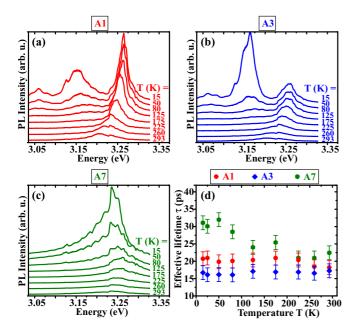| sample	doping density n_D (cm^{-3})	β-GaN thickness (nm)	β-AlN buffer thickness (nm)	substrate
A1	1×10^{17}	580	30	12 μm 3C-SiC/Si(001)
A2	5×10^{17}	580	15	12 μm 3C-SiC/Si(001)
A3	1×10^{18}	580	15	12 μm 3C-SiC/Si(001)
A4	5×10^{18}	580	30	12 μm 3C-SiC/Si(001)
A5	5×10^{18}	580	15	12 μm 3C-SiC/Si(001)
A6	1×10^{19}	580	39	12 μm 3C-SiC/Si(001)
A7	1.5×10^{19}	580	39	12 μm 3C-SiC/Si(001)
B1	1×10^{17}	100	no AlN buffer	9 μm 3C-SiC/Si(001)
B2	5×10^{17}	500	no AlN buffer	9 μm 3C-SiC/Si(001)
B3	1×10^{18}	500	no AlN buffer	9 μm 3C-SiC/Si(001)
C	6×10^{16}	400	no AlN buffer	30 nm 3C-SiC/Si(001)
D	8×10^{17}	970	no AlN buffer	GaAs(001)

FIG. 1. (a)–(c) Temperature dependent PL spectra for samples A1, A3, and A7. (d) Temperature dependence of the effective lifetime τ of the excitonic PL line.
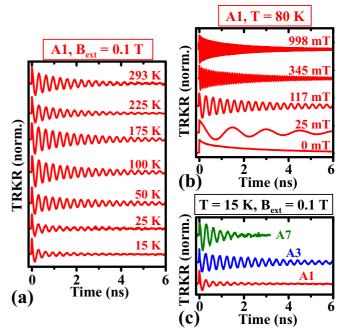

FIG. 2. TRKR transients for sample A1 for (a) different temperatures and (b) different external magnetic fields. (c) TRKR transients for samples A1, A3, and A7 at $T = 15$ K.

IV. EXPERIMENTAL RESULTS AND DISCUSSION

In the following section, we will present and discuss the experimental results, starting first with the PL characterization of the samples, before discussing the dependence of spin relaxation on temperature, magnetic field, and doping density. Finally, we address shortly the influence of phase purity and substrate on the spin dynamics.

A. Photoluminescence

Figures 1(a)–1(c) shows typical PL spectra of samples A1, A3 and A7 for different temperatures. The PL spectra of samples A1 and A3 are dominated by luminescence lines at 3.26 eV and 3.144 eV at low temperatures. The PL line at 3.144 eV stems from a donor-acceptor-pair transition (DAP) with its LO phonon replica at 3.057 eV. For temperatures $\geqslant 50$ K, the DAP line is superseded by the band-acceptor transition (e, A^0) approximately 25 meV higher in energy [55]. Similarly, the luminescence line at 3.26 eV originates from the radiative decay of donor-bound-excitons (D^0, X) at low temperatures, and is gradually replaced by recombination of free excitons (FX) at higher temperatures [56]. The full width at half maximum (FWHM) of the excitonic line of, e.g., 25 meV for sample A1 at a temperature of $T = 15$ K, compares well with values in the literature [56,57], thus demonstrating the good quality of the samples. With increasing temperature, the PL lines redshift due to the temperature-induced band-gap shrinking, accompanied by an intensity decrease and broadening of the lines. The short effective lifetime of the excitonic PL line on the order of 20 ps [cf. Fig. 1(d)] shows that recombination is predominantly nonradiative consistent with the decrease in intensity.

The PL spectrum of the highly n-doped sample A7 [see Fig. 1(c)] shows a broad, asymmetric PL line shape [58] typical

for degenerate bulk semiconductors due to band-to-band transitions or recombination of free electrons with localized hole states [49]. For increasing temperature, the line shape broadens and evolves into a more symmetric line shape, resulting in an almost Gaussian form at room temperature due to thermal excitation and broadening effects [59].

B. Temperature dependence of spin dynamics

First, we will discuss the temperature dependence of spin relaxation. Figure 2(a) shows typical TRKR transients for sample A1 at different temperatures in an external magnetic field $B_{\mathrm{ext}} = 0.1$ T. The transients show oscillations, which are caused by Larmor precession of the electron spins around the external magnetic field, and a temporal decay of the amplitude due to spin relaxation and generally also due to the decay of the optically excited carrier density. The corresponding Larmor precession frequency ω_L and the spin-relaxation time τ_s are extracted from the transients by fits of the form $[A_1 \exp(-t/\tau_c) + A_2 \exp(-t/\tau_s) \cos[\omega_L(t - t_0)]$, where the time τ_c accounts for the decay of the optically excited carrier density [11]. Here, τ_c is found to approximately equal the effective decay time τ (compare Sec. IV A) and to be short as compared to the spin-relaxation time τ_s for all measurements. Carrier densities are therefore virtually constant on the timescale of spin relaxation. The Larmor precession frequency ω_L is related to the electron Landé g factor via $\omega_L = g\mu_B B_{\mathrm{ext}}/\hbar$. We find a g factor $g \approx 1.95$ in agreement with the literature value [60]. Within experimental accuracy, the g factor is independent of temperature and doping level for all investigated samples in complete agreement with expectations from $\mathbf{k} \cdot \mathbf{p}$ theory for the combination of large band gap and small spin-orbit coupling in β-GaN [61].
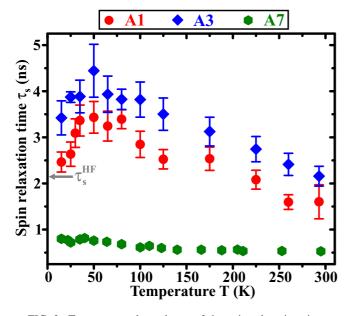
FIG. 3. Temperature dependence of the spin-relaxation time τ_s for samples A1, A3, and A7 in an external magnetic field $B_{\text{ext}} = 0.1$ T. The gray arrow marks the spin-relaxation time τ_s^{HF} due to the hyperfine interaction estimated via Eq. (17).

The temperature dependence of the spin-relaxation time τ_s is shown in Fig. 3. Two temperature regimes are clearly observed for the two lower doped samples A1 and A3. At temperatures $T \leqslant 50$ K, the spin-relaxation time increases with T, while a decrease of τ_s with T is observed for $T \geqslant 50$ K. In contrast, the highly doped sample A7 shows an almost constant spin relaxation time as reported previously [19].

First, we will discuss the nonmonotonic temperature dependence of spin relaxation in samples A1 and A3, which can be explained by the combined action of hyperfine-induced spin relaxation of localized electrons and DP relaxation of delocalized electrons. At low temperatures, a substantial fraction of electrons is localized at defects, and hyperfine-induced spin relaxation dominates, while DP relaxation is comparably inefficient at low temperatures. With increasing temperature, both the fraction of delocalized electrons as well as the efficiency of DP relaxation increase, resulting in the dominance of DP relaxation at high temperatures.

For the low-temperature regime, where the spin relaxation of localized electrons via hyperfine interaction dominates, we estimate a spin-relaxation time $\tau_s^{\text{HF}} \approx 2.1$ ns according to Eq. (17). The effect of the N nuclei is neglected as compared to the Ga nuclei [62], for which a hyperfine constant $A_{\text{Ga}} = 42$ μeV averaged over the ^{69}Ga and ^{71}Ga isotopes is used [62,63]. The estimated spin-relaxation time is in good agreement with the experimentally found values for the lowest temperature of $T = 15$ K (compare the gray arrow marking τ_s^{HF} in Fig. 3). The experimentally observed increase of the spin-relaxation time with temperature then follows from increasing delocalization and hence increasing contribution from slow DP relaxation. The overall longer spin-relaxation times for sample A3 with its higher doping level as compared to sample A1 are again expected as a consequence of the smaller fraction of localized carriers.

In the high-temperature regime of spin relaxation, the experimentally observed decrease of the spin-relaxation time with temperature can be explained by the dominance of DP relaxation. The increasing temperature leads to the occupation of higher k states and a corresponding increase of the effective magnetic field [see Eq. (3)], resulting finally in faster spin relaxation. For a quantitative comparison of the predictions of DP theory to the experimentally observed temperature dependence of spin relaxation, both the effective magnetic field average and the momentum scattering time have to be known according to Eqs. (4) to (12). The experimental determination of the momentum scattering time via transport measurements is, however, often hindered in β-GaN due to the use of highly conductive substrates. In addition, an experimentally measured total momentum relaxation time does not account for the different efficiencies of the individual momentum scattering processes [cf. Eq. (5)] [64]. We therefore model the momentum scattering time in the following, thus allowing us to include the different efficiencies of the individual momentum scattering mechanisms as discussed in Sec. II A. Generally, the transport mobility μ_e is linked to the momentum scattering time τ_p via $\tau_p = \mu_e m^*/q$. We model the total mobility μ_e in the following by including several scattering processes via Matthiessens rule

$$\frac{1}{\mu_e} = \frac{1}{\mu_e^{\text{disl}}} + \frac{1}{\mu_e^{\text{po}}} + \frac{1}{\mu_e^{\text{dp}}} + \frac{1}{\mu_e^{\text{ii}}} + \frac{1}{\mu_e^{\text{pe}}} , \quad (23)$$

where the mobility μ_e^{disl} due to dislocation scattering is given by [65,66]

$$\mu_e^{\text{disl}}(T, n_D) = \frac{30\sqrt{2\pi}\varepsilon^2 d^2 (k_B T)^{3/2}}{q^3 \lambda_D f^2 \sqrt{m^*} n_{\text{disl}}} \quad (24)$$

with n_{disl} as the dislocation density, d as the distance between acceptor centers along the dislocation line, f as the occupation ratio of these acceptors and

$$\lambda_D = \sqrt{\frac{\varepsilon k_B T}{q^2 n_D}} \quad (25)$$

as the Debye screening length. For the simulations, it was assumed that d is equal to the lattice constant a_0 of β-GaN and f is equal to 1 [67]. The mobility μ_e^{po} due to scattering with polar optical phonons is modeled by [68]

$$\mu_e^{\text{po}} = \frac{8}{3\sqrt{2\pi}} \frac{\hbar^2 (k_B T)^{1/2}}{q k_B T_{\text{LO}} m^{*3/2}} \frac{\varepsilon \varepsilon_\infty}{\varepsilon - \varepsilon_\infty} (e^\Theta - 1)\chi(\Theta) \quad (26)$$

with $\Theta = T_{\text{LO}}/T$, $T_{\text{LO}} = \hbar\omega_{\text{LO}}/k_B$ and

$$\chi(\Theta) = \tfrac{3}{8}\sqrt{\pi\Theta} \quad (27)$$

for $T_{\text{LO}} \gg T$. The mobility μ_e^{dp} due to acoustic phonon deformation potential scattering is given by [43,69]

$$\mu_e^{\text{dp}} = \frac{\sqrt{8\pi}}{3} \frac{q\hbar^4 c_l}{a_c^2 m^{*5/2} (k_B T)^{3/2}} \quad (28)$$

with the deformation potential a_c and the spherically averaged [70]

$$c_l = (3c_{11} + 2c_{12} + 4c_{44})/5 . \quad (29)$$

Scattering with ionized impurities leads to the mobility [71]

$$\mu_e^{\mathrm{ii}} = \frac{128\sqrt{2\pi}\,\varepsilon^2 (k_B T)^{3/2}}{m^{*1/2} q^3 n_D} \left[\ln\left(1 + \frac{(12\pi\varepsilon k_B T)^2}{q^4 n_D^{2/3}} \right) \right]^{-1}.$$

(30)

The mobility due to piezoelectric scattering is given by [43]

$$\mu_e^{\mathrm{pe}} = \frac{140\sqrt{2\pi}}{3} \frac{\hbar^2}{q m^{*3/2} (k_B T)^{1/2}} \frac{1}{h_{14}^2 (4/c_t + 3/c_l)}$$

(31)

with the spherically averaged parameter [70]

$$c_t = (c_{11} - c_{12} + 3c_{44})/5$$

(32)

and [72]

$$h_{14} = e_{14}/\varepsilon.$$

(33)

Figure 4(a) shows exemplarily the contributions from the different scattering mechanisms to the total mobility μ_e for
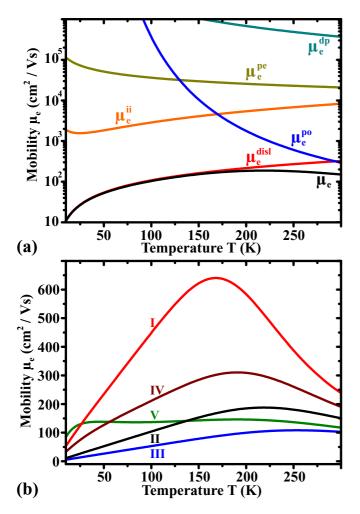

(a)

(b)

FIG. 4. Simulated temperature dependence of (a) the contributions of the different scattering mechanisms to the total mobility μ_e for $n_D = 1 \times 10^{17}$ cm^{-3} and $n_{\mathrm{disl}} = 5 \times 10^9$ cm^{-2} and (b) the total mobility μ_e for $n_D = 1 \times 10^{17}$ cm^{-3} and $n_{\mathrm{disl}} = 1 \times 10^9$, 5×10^9, and 5×10^{10} cm^{-2} (lines I–III). Lines IV and V are for doping densities of 1×10^{18} and 1×10^{19} cm^{-3} and a dislocation density of $n_{\mathrm{disl}} = 5 \times 10^9$ cm^{-2}.

TABLE V. Material parameters of cubic GaN.

	Symbol	Value	Reference
Spin orbit splitting	Δ_{so}	0.017 eV	Ref. [74]
Effective electron mass	m^*	0.15 m_0	Ref. [75]
LO phonon frequency	$\tilde{\nu}_{\mathrm{LO}}$	740 cm^{-1}	Ref. [76]
Static dielectric constant	ε	9.5 ε_0	Ref. [67]
High-frequency dielectric constant	ε_∞	5.35 ε_0	Ref. [67]
Lattice constant	a_0	0.45 nm	Ref. [77]
Deformation potential	a_c	−2.77 eV	Refs. [78,79]
Elastic constant	c_{11}	296 GPa	Ref. [78]
Elastic constant	c_{12}	154 GPa	Ref. [78]
Elastic constant	c_{44}	206 GPa	Ref. [78]
Piezoelectric constant	e_{14}	0.50 C/m^2	Ref. [80]

a doping density $n_D = 1 \times 10^{17}$ cm^{-3} and a typical value [73] of the dislocation density of $n_{\mathrm{disl}} = 5 \times 10^9$ cm^{-2}, using the material parameter given in Table V. The total mobility is dominated by dislocation scattering at low temperatures and by polar optical phonon scattering at high temperatures, while ionized-impurity scattering gains importance with increasing doping level. The dislocation density n_{disl} and the doping density n_D are therefore the sample specific parameters governing the mobility. The temperature dependence of the total mobility is shown in Fig. 4(b) for the range of doping densities n_D investigated here and for values of the dislocation density covering the typical range found for our samples with a layer thickness of approximately 500 nm on SiC substrates [73]. Overall, the simulated values of the mobility agree well with available experimental values for the mobility in β-GaN [51,67,81].

In the next step, the contributions of the individual scattering mechanisms to the total scattering time can be weighted by their corresponding efficiency factors, thus allowing a quantitative comparison between the experimental spin-relaxation times and the predictions of DP theory.

We start by discussing the two lower doped samples A1 and A3. Figure 5(a) shows the simulated temperature dependence of the weighted effective momentum scattering time $(Q\tau_p)_{\mathrm{total}}$ according to Eq. (9) for the doping densities of samples A1 and A3, assuming a typical dislocation density of $n_{\mathrm{disl}} = 5 \times 10^9$ cm^{-2}. Following Eq. (7), the product $\tau_s (Q\tau_p)_{\mathrm{total}}$ of the experimentally determined spin-relaxation time τ_s and the simulated $(Q\tau_p)_{\mathrm{total}}$ can then be directly compared to the inverse effective magnetic field average $1/\langle\Omega_{\mathrm{eff,nd}}^2\rangle$ predicted by DP theory [cf. Eq. (8)]. Figure 5(b) shows the corresponding comparison between $\tau_s (Q\tau_p)_{\mathrm{total}}$ and $1/\langle\Omega_{\mathrm{eff,nd}}^2\rangle$ for different values of the spin-splitting constant γ_e and temperatures up to 500 K [82]. Qualitatively, the slope of $\tau_s (Q\tau_p)_{\mathrm{total}}$ matches the T^{-3} dependence predicted by DP theory [see Eq. (8)] very well for temperatures $T \gtrsim 250$ K for both samples. Quantitative agreement is, however, only obtained for a value of $\gamma_e = 2.5$ eVÅ^3, which strongly exceeds the published theoretical values (see Table II). The significantly shorter spin-relaxation times for lower temperatures $T \lesssim 250$ K can be understood by increasing degeneracy for lower temperatures and strong contribution from spin relaxation of localized carriers.
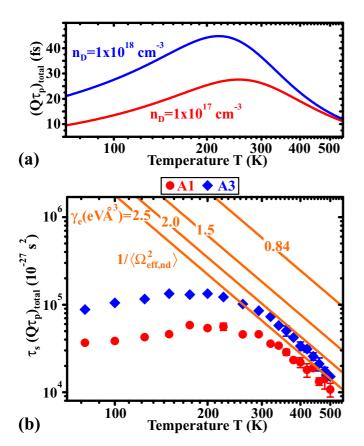
FIG. 5. (a) Simulated temperature dependence of the weighted momentum scattering time $(Q\tau_p)_{total}$ according to Eq. (9) for a dislocation density $n_{disl} = 5 \times 10^9$ cm^{-2} and doping densities $n_D = 1 \times 10^{17}$ and 1×10^{18} cm^{-3}, respectively. (b) Temperature dependence of the product $\tau_s(Q\tau_p)_{total}$ of the experimental spin-relaxation time τ_s and $(Q\tau_p)_{total}$ from 80 to 500 K on a double-logarithmic scale. The solid lines show the inverse squared effective magnetic field average $1/\langle\Omega^2_{eff,nd}\rangle$ predicted by DP theory for different values of the spin-splitting constant γ_e.

An analogous comparison can be made for the degenerately doped sample A7. In this case, the effective magnetic field average $\langle\Omega^2_{eff,deg}\rangle$ and the effective momentum scattering time $\tau_{p,eff}^{deg}$ according to Eqs. (13) and (14) have to be used to account for the degeneracy. Figure 6(a) shows the simulated temperature dependence of $\tau_{p,eff}^{deg}$, which is approximately constant as expected for a degenerate electron gas [1]. The product $\tau_s\tau_{p,eff}^{deg}$ is then also found to be almost temperature independent, which completely agrees with the prediction of DP theory for the case of degeneracy [cf. Fig. 6(b)] [3,19]. This agreement clearly indicates the dominance of DP relaxation over the full temperature range due to the degeneracy of the sample. Consistent with the above results for the lower doped samples, quantitative agreement with DP theory is again obtained for a value of the spin-splitting constant of $\gamma_e = 2.5$ eVÅ^3.

This value of the spin-splitting constant is, however, substantially larger than published theoretical values (see Table II). In the following, we will discuss possible reasons for this discrepancy. An obvious reason for the disagreement would be a too small value of γ_e predicted by theory. It
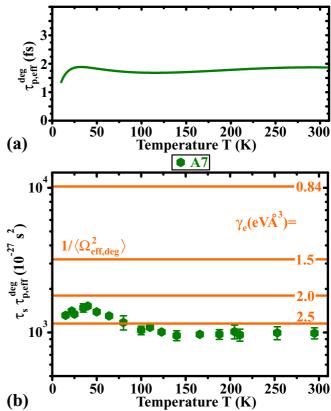

FIG. 6. (a) Simulated temperature dependence of the effective momentum scattering time $\tau_{p,eff}^{deg}$ according to Eq. (14) for a doping density $n_D = 1.5 \times 10^{19}$ cm^{-3} and a dislocation density $n_{disl} = 5 \times 10^9$ cm^{-2}. (b) Temperature dependence of $\tau_s\tau_{p,eff}^{deg}$ from 15 K up to 293 K on a semi-logarithmic scale. The solid lines show the inverse squared effective magnetic field average $1/\langle\Omega^2_{eff,deg}\rangle$ predicted by DP theory for different values of the spin-splitting constant γ_e.

is well known from other semiconductors, particularly from the extensively studied GaAs, that the theoretical prediction of the spin-splitting constant is difficult, resulting in a wide range of predicted values [83]. The few theoretically predicted values for γ_e in β-GaN also show considerable scatter (cf. Table II), with, however, a tendency to smaller values for increased complexity of the theoretical models [19,32,33]. We note that no experimental values for the spin-splitting constant in β-GaN are available for comparison. Another reason for the observed discrepancy might be the assumption of a perfect crystal lattice in the theoretical prediction of γ_e. Cubic GaN possesses, however, a complex microstructure, which possibly influences the spin dynamics in several ways. First, cubic GaN shows inclusions of the thermodynamically preferred wurtzite phase of GaN (α-GaN), arising from stacking faults on {111} planes. These α-GaN inclusions furthermore form two types of anti-phase domains (APD) in β-GaN grown on 3C-SiC, with different α-GaN content in the two types of APDs [84]. This complex phase mixture could lead to additional contributions to DP spin relaxation, as the polar α-GaN inclusions and the charge accumulation at the interfaces [85] might contribute to random spin-orbit coupling similar to dopant ions [86]. We note that while HRXRD characterizations indicate a high phase purity and thus a small amount of α-GaN domains in

our samples, these measurements only provide information averaged over the whole layer thickness, while in reality the α-GaN phase content increases with increasing layer thickness [84]. Due to the short laser penetration depth, our TRKR measurements probe predominantly the electron spin dynamics close the surface, where the α-GaN phase content is expected to be higher than indicated by the HRXRD measurement. Besides α-GaN inclusions, cubic GaN epilayers show also a high density of dislocations, which might influence DP relaxation via two, counteracting mechanisms. On the one hand, an increasing dislocation density causes shorter momentum scattering times as discussed above, thus leading to an increase of the spin-relaxation time. On the other hand, dislocations in GaN are positively charged [87], thus creating an additional spin-orbit field comparable to the spin-orbit field of donors [86], which leads to shorter spin lifetimes for increasing dislocation density. While only the first mechanism has theoretically been considered so far [28], experimental results in α-GaN point at the possible importance of the second mechanism [88].

A significant underestimation of the mobility and hence the momentum scattering time in our simulations could also explain the shorter spin-relaxation times observed experimentally than expected theoretically. The simulated mobilities agree, however, well with available experimental values [51,67,81]. In addition, electron-electron scattering also shortens the momentum scattering time for DP relaxation, while it does not contribute to the transport mobility. Inclusion of electron-electron scattering would

hence increase the gap between experiment and theory even further.

Microstrain variations in the β-GaN epilayers lead to an additional contribution to the conduction band spin splitting. The strain-induced spin splitting was, however, shown to have only a negligible effect on the spin dynamics [89], thus excluding strain variations as a possible source for the discrepancy.

We finally note that EY and BAP relaxation play only a negligible role. Estimating spin-relaxation times for EY relaxation via Eq. (21) gives values on the order of microseconds, being several orders of magnitude longer than the experimentally observed spin-relaxation times. A significant influence of BAP relaxation is not expected, as the BAP mechanism was shown to be effective only for considerable hole concentrations [1,2], while our samples are n-doped and holes optically excited by the pump pulse recombine rapidly (see Sec. IV A).

C. Magnetic field dependence of spin dynamics

The investigation of the magnetic field dependence of spin relaxation gives important information on, e.g., the symmetry of the spin-relaxation tensor [10,20] or on the dominating spin-relaxation mechanism [13]. Figure 7 shows the magnetic field dependence of spin relaxation for the lower doped samples A1 and A3 as well as for the degenerate sample A7 at temperatures between 15 and 293 K. First, we will discuss the magnetic field dependence of the spin-relaxation time for the two lower doped samples A1 and A3. At low temperatures, the spin-
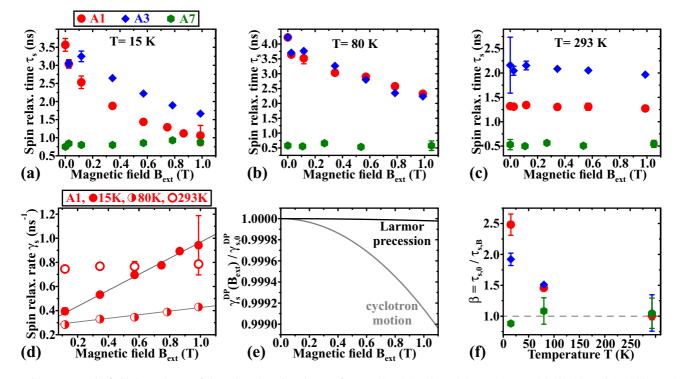

FIG. 7. Magnetic field dependence of the spin-relaxation time τ_s for samples A1, A3, and A7 at (a) $T = 15$, (b) 80, and (c) 293 K. (d) Magnetic field dependence of the corresponding spin-relaxation rate γ_s for sample A1 at $T = 15$, 80, and 293 K. The solid lines show fits to the $\gamma_s \propto B_{ext}$ dependence of Eq. (20). (e) Simulated magnetic field dependence $\gamma_s^{DP}(B_{ext})/\gamma_{s,0}^{DP}$ of the ratio of spin-relaxation rates due to the effects of Larmor precession and cyclotron motion, respectively, according to Eqs. (15) and (16). An effective momentum scattering time $\tau_p = 25$ fs was used in the simulation. (f) Temperature dependence of the ratio $\beta = \tau_{s,0}/\tau_{s,B}$ of experimental spin-relaxation times at zero magnetic field and $B_{ext} = 0.55$ T for samples A1, A3, and A7. The dashed line marks a value of $\beta = 1$, indicative of DP relaxation.

relaxation time strongly decreases for increasing magnetic field [cf. Fig. 7(a)]. The linear magnetic field dependence of the corresponding spin-relaxation rate [see Fig. 7(d)] is typical for the spin relaxation of localized electrons [cf. Eq. (20)]. The magnetic field dependence of the spin-relaxation time flattens with increasing temperature, resulting in an almost constant spin-relaxation time at room temperature [compare Figs. 7(b)–7(d)]. This transition supports the interpretation of the temperature dependence of spin relaxation in the previous section. At low temperatures, spin relaxation is governed by the spin relaxation of localized electrons via the hyperfine interaction, which is characterized by the linear magnetic field dependence of the spin-relaxation rate that we experimentally observe for sample A1 and A3. With increasing temperature, the degree of localization decreases and the efficiency of DP relaxation increases simultaneously, leading to the dominance of DP relaxation at room-temperature. DP relaxation is essentially independent of the external magnetic field for the field range investigated here, as cyclotron motion and Larmor precession around the external magnetic field lead only to a minute modification of the spin-relaxation rate [see Fig. 7(e)]. Due to the different magnetic field dependencies of spin relaxation of localized electrons and DP relaxation, the ratio $\beta = \tau_{s,0}/\tau_{s,B}$ of the experimental spin-relaxation times $\tau_{s,0}$ in zero magnetic field and $\tau_{s,B}$ in a finite magnetic field $B_{ext} = 0.55$ T can be used as a probe for the importance of localization for spin relaxation [13]. For the spin relaxation of localized electrons, $\beta > 1$ follows, while DP relaxation corresponds to $\beta = 1$. The temperature dependence of β shown in Fig. 7(f) illustrates the transition from spin relaxation dominated by localized electrons to DP dominated spin relaxation at room temperature.

Additional evidence for the important influence of localized electrons on spin relaxation even up to room temperature comes from the magnetic field dependent measurement of spin relaxation shown in Fi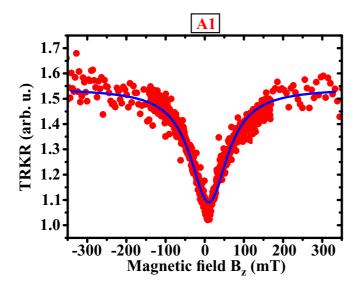g. 8 for sample A1 where, similar to resonant spin amplification (RSA) measurements, the external magnetic field is scanned for a fixed time delay Δt between pump and probe pulse. The external magnetic field B_z is oriented perpendicular to the sample plane in this measurement (Faraday configuration). The observed increase of spin polarization for moderate external fields B_z is typical for localized electrons subject to hyperfine-induced spin relaxation and can be understood as a suppression of the fluctuating hyperfine field by the external field, with the half width at half minimum of the peak as a direct measure of the hyperfine field B_{hf} [90]. Approximating the dip by a Lorentzian [37,90]

$$A_{\text{Far}}(B_{ext}) = A_0\left[1 - \frac{2A_1/3}{1 + (B_z/B_{hf})^2}\right] \quad (34)$$

gives $B_{hf} \approx 57.7$ mT. According to

$$\tau_s = 2\sqrt{3}\hbar/(g\mu_B B_{hf}) \quad (35)$$

a spin dephasing time $\tau_s \approx 0.35$ ns follows [37], supporting the assumption of a significant contribution of localized electrons to the total spin relaxation up to room temperature. The shorter spin-relaxation time of localized electrons at room temperature as compared to low temperatures is expected, particularly due to the stronger localization at deep defects and phonon-induced dephasing [91]. We note that deep states with strongly localized wave functions are well-known to be present in β-GaN from PL measurements [57,92].

Finally, we discuss the magnetic field dependence of the degenerately doped sample A7. For this sample, spin relaxation is found to be almost independent of the magnetic field over the whole temperature range [see Figs. 7(a)–7(c) and 7(e)]. This flat magnetic field dependence with $\beta \approx 1$ [cf. Fig. 7(f)] clearly demonstrates that DP relaxation is dominating due to the degeneracy and the correspondingly small degree of localization in this sample. This finding is in complete agreement with the conclusion from the temperature dependence in the previous section.

D. Doping density dependence of spin dynamics

The dependence of spin relaxation on the doping density gives additional important information complementary to the information from temperature or magnetic field dependent measurements, for example on the dominating spin-relaxation mechanism or on the leading contribution to DP relaxation [12,39]. Figure 9 shows the doping density dependence of the spin-relaxation time for ten samples with doping densities $n_D = 6 \times 10^{16}$–1.5×10^{19} cm^{-3} at temperatures of 80 and 293 K, respectively. A nonmonotonic density dependence of the spin-relaxation time is found at both temperatures, with a maximum spin lifetime at an intermediate density of 10^{18} cm^{-3}. In the following, we will show that the observed density dependence can again be understood by the interplay of spin relaxation of localized electrons and DP relaxation of free electrons.

Generally, the doping density influences the spin dynamics in a complex way, as it determines via the degree of localization not only the relative importance of spin relaxation of localized and delocalized electrons, respectively, but also the absolute efficiency of spin-relaxation mechanisms in the two regimes. We will therefore first discuss the doping density dependence
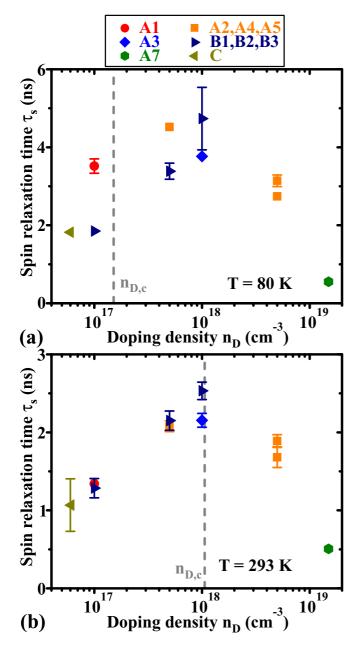

FIG. 8. Magnetic field dependence of the spin polarization in Faraday configuration for sample A1 at a temperature of $T = 293$ K and a time delay $\Delta t = 2.1$ ns between pump and probe pulse. The solid line shows a fit according to Eq. (34).

(a)

(b)

FIG. 9. Doping density dependence of the spin-relaxation time τ_s at temperatures of (a) $T = 80$ K and (b) $T = 293$ K for doping densities from $n_D = 6 \times 10^{16}$ cm^{-3} up to 1.5×10^{19} cm^{-3} in an external magnetic field of $B_{\text{ext}} = 0.1$ T.

of the different spin-relaxation mechanisms in more detail, starting with the spin relaxation of localized electrons. For small densities of localized electrons with correspondingly large separations between neighboring electrons, the localized electrons do not interact with each other and a density-independent spin-relaxation rate γ_s^{HF} according to Eq. (17) results. A pronounced density dependence occurs, however, at higher densities for electrons localized at donors, where exchange between the donor-bound electrons strongly increases with doping density [34]. In this case, spin relaxation both due to hyperfine interaction as well as due to anisotropic exchange interaction depends on the correlation time τ_c [see Eqs. (18) and (19)], which strongly decreases with doping density.

A nonmonotonic density dependence with maximum spin lifetime at an intermediate density results, as spin relaxation due to the hyperfine interaction slows down with increasing density, while spin relaxation due to anisotropic exchange speeds up with density [34,39]. To compare the predicted density dependence to the experimental results, we calculate the spin-relaxation rates $\gamma_s^{\text{HF,h}}$ due to hyperfine interaction according to Eq. (18) and γ_s^{aex} due to anisotropic exchange according to Eq. (19). The correlation time τ_c is estimated via [39]

$$\tau_c \approx \hbar/\xi J(r_c) , \qquad (36)$$

where the exchange constant $J(r)$ is approximated in analogy to hydrogenic systems by [39,93]

$$J(r) = 0.821 E_B \left(\frac{r}{a_B} \right)^{5/2} e^{(-2r/a_B)} . \qquad (37)$$

The average characteristic distance r_c between interacting donors is assumed to be

$$r_c = \zeta n_D^{-1/3} . \qquad (38)$$

The prefactor ζ is estimated either from the maxima of distribution functions of the distance to the nearest neighbors or from percolation theory [34]. The numerical factor ξ is of the order of one. We use the values $\zeta = 0.65$ and 0.8 following from experimental data for GaAs at low temperatures [39]. The mean-squared value of the angle of spin rotation φ in Eq. (19) is numerically approximated by [39]

$$\langle \varphi^2(r) \rangle^{1/2} = \frac{\sqrt{2}\gamma_e}{E_B a_B^3} \left[0.323 + 0.436 \left(\frac{r}{a_e} \right) + 0.014 \left(\frac{r}{a_e} \right)^2 \right] \qquad (39)$$

with the modified Bohr radius a_e defined as above and the approximate binding energy $E_B = E_{B,H}(m^*/m_0)/(\varepsilon/\varepsilon_0)^2$, where $E_{B,H}$ is the Rydberg energy of an H atom. Figure 10 shows the corresponding simulated density dependence, where spin relaxation is limited for small donor concentrations by the relaxation of isolated electrons. The resulting total spin-relaxation time shows indeed a nonmonotonic density dependence. The predicted spin-relaxation times exceed, however, the experimentally found spin-relaxation times by almost two orders of magnitude. In addition, the predicted density for maximum spin lifetimes is smaller than the experimentally observed density by a factor of 20. These findings clearly rule out the density dependence due to donor-bound electrons as an explanation for the observed density dependence of spin relaxation.

Next, we will discuss the density dependence in the regime of DP relaxation of delocalized electrons, where both the magnitude of the effective magnetic field and the momentum scattering time depend on the doping density. Generally, two regimes of spin relaxation exist in the majority of bulk III-V semiconductors, leading again to a nonmonotonic density dependence with maximum spin-relaxation time at an intermediate density [2,12]. The two regimes can conveniently be characterized by the ratio of the lattice temperature T to the Fermi temperature T_F, where the Fermi temperature $T_F = E_F/k_B$ is determined by the doping density n_D via the Fermi
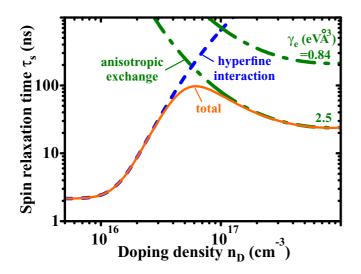
FIG. 10. Simulated doping density dependence of the spin-relaxation times of donor-bound electrons due to hyperfine interaction (dashed line) and due to anisotropic exchange (dash-dotted line), together with the resulting total spin-relaxation time (solid line) for a value of the spin-splitting constant of $\gamma_e = 2.5 \, \text{eV\AA}^3$. For comparison, the spin-relaxation time due to anisotropic exchange is also shown for $\gamma_e = 0.84 \, \text{eV\AA}^3$.

energy $E_F = (3\pi^2)^{2/3}\hbar^2 n_D^{2/3}/2m^*$. For lattice temperatures $T \gg T_F$ well exceeding the Fermi temperature, the electron system is nondegenerate and the effective magnetic field average is approximately independent of the doping density. Usually, momentum scattering is dominated by ionized impurity scattering and electron-electron scattering in bulk III-V semiconductors, for which the momentum scattering time decreases with doping density. Overall, the spin-relaxation time then increases with density in the nondegenerate regime for the majority of III-V semiconductors. In β-GaN, however, momentum scattering is dominated by dislocation scattering, which weakens for increasing doping density. The total momentum scattering time is therefore expected to moderately increase with doping density, leading to a slightly decreasing spin-relaxation time in the nondegenerate regime. In the second regime, where the Fermi temperature exceeds the lattice temperature ($T_F \gg T$), the electron system is degenerate. The effective magnetic field average rapidly grows with doping density in this regime as higher k states get populated. The momentum scattering time is, on the other hand, almost constant in the degenerate regime, hence the spin-relaxation time decreases with density in the degenerate regime. Overall, a nonmonotonic density dependence is expected to result from these two regimes with a maximum spin lifetime at a critical density $n_{D,c}$, for which the Fermi temperature $T_F(n_{D,c}) \approx T$ is comparable to the lattice temperature T [2]. For β-GaN with strong dislocation scattering, a transition from an almost constant or slightly decreasing spin-relaxation time to the pronounced decrease in the degenerate regime is expected at the critical density $n_{D,c}$.

Here, critical densities of $n_{D,c} = 1.5 \times 10^{17}$ and $1.06 \times 10^{18} \, \text{cm}^{-3}$, respectively, correspond to the investigated temperatures of $T = 80$ and 293 K. The experimentally observed density dependence therefore clearly deviates from

the predicted DP density dependence for $T = 80$ K, as a pronounced increase of the spin-relaxation time is found in the nondegenerate regime and the density for maximum spin lifetime in addition strongly deviates from the predicted $n_{D,c}$ [see dashed line in Fig. 9(a)]. At $T = 293$ K, the experimental density for maximum spin lifetime coincides with the predicted critical density $n_{D,c}$ [see dashed line in Fig. 9(b)], the pronounced increase of the spin-relaxation time for nondegenerate densities does, however, not agree with the expected density dependence for β-GaN.

Following the above discussion, the experimentally observed density dependence can be understood neither by spin relaxation of localized electrons nor by DP relaxation alone, but only by the combined spin relaxation of localized and delocalized electrons. For low densities $n_D \lesssim 10^{18} \, \text{cm}^{-3}$, spin relaxation of electrons localized at deep states strongly contributes to the total spin relaxation. Increasing density leads to a stronger contribution from comparably weak DP relaxation, resulting in an increase of the total spin-relaxation time with density. For high densities, DP relaxation dominates due to the small degree of localization and the strongly increased efficiency of the DP mechanism. The spin-relaxation time shows the corresponding drastic decrease with density being typical for DP relaxation in the degenerate regime. The comparison between the density dependence of the product $\tau_s \tau_{p,\text{eff}}^{\text{deg}}$ of the experimental spin-relaxation time τ_s and the simulated effective momentum scattering time $\tau_{p,\text{eff}}^{\text{deg}}$ with the inverse squared effective magnetic field average $1/\langle \Omega_{\text{eff,deg}}^2 \rangle$ predicted by DP theory for degenerate electrons strongly supports this interpretation, as good agreement is found for samples A4, A5, and A7 for both temperatures of 80 and 293 K (see Fig. 11).
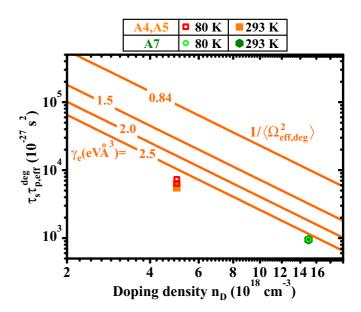

FIG. 11. Doping density dependence of the product $\tau_s \tau_{p,\text{eff}}^{\text{deg}}$ of the experimental spin-relaxation time τ_s and the simulated effective momentum scattering time $\tau_{p,\text{eff}}^{\text{deg}}$ in the degenerate regime at temperatures of $T = 80$ and 293 K. The solid lines show the inverse squared effective magnetic field average $1/\langle \Omega_{\text{eff,deg}}^2 \rangle$ predicted by DP theory for different values of the spin-splitting constant γ_e.
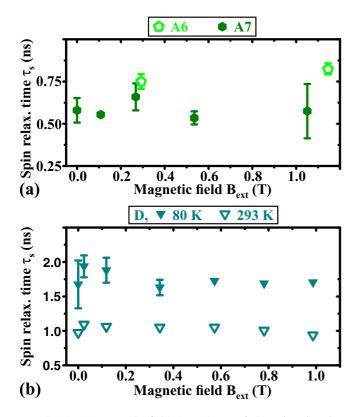
FIG. 12. (a) Magnetic field dependence of the spin-relaxation time at $T = 80$ K for sample A6 with 97.5% phase purity and sample A7 with 99.7% phase purity. (b) Magnetic field dependence of the spin-relaxation time at $T = 80$ and 293 K, respectively, for sample D grown on GaAs substrate.

E. Influence of hexagonal phase content and substrate on the spin dynamics

The investigated β-GaN epilayers possess a complex microstructure which potentially has a strong influence on the spin dynamics as discussed above. In the remaining, we will briefly present additional measurements on the influence of the phase mixture of cubic and hexagonal crystal phases as well as of dislocations. First, the spin dynamics of the degenerately doped samples A6 and A7 is compared. Both samples have the same doping level and layer structure, but different phase purities of 97.5% and 99.7%, respectively (see Table IV). Figure 12(a) shows the magnetic field dependence of spin relaxation for both samples at a temperature of $T = 80$ K. The spin-relaxation time is almost independent of the magnetic field for both samples, indicating the dominance of DP relaxation as a consequence of degeneracy. Moreover, the spin-relaxation times approximately agree for the two samples. The almost identical spin dynamics in both samples despite their substantially different phase purity suggests an only marginal influence of the hexagonal phase. More in-depth studies are, however, required for a conclusive statement on the role of phase mixture for the dynamics of spin relaxation.

Finally, we investigate the possible influence of dislocations. For this purpose, we study the spin dynamics in a sample grown on GaAs substrate (sample D with a doping

density of $n_D = 8 \times 10^{17}$ cm^{-3}), as β-GaN epilayers grown on GaAs substrates generally have higher dislocation densities than comparable layers grown on 3C-SiC [73]. Figure 12(b) shows the magnetic field dependence of spin relaxation for sample D at temperatures of $T = 80$ and 293 K. The spin dynamics differs in two aspects from the spin dynamics of comparable samples on 3C-SiC, which were discussed before (cf. Fig. 7). First, sample D shows an almost flat magnetic field dependence already at $T = 80$ K, while the magnetic field dependence flattens out only at 293 K in comparable samples grown on SiC. Second, the spin-relaxation times are shorter for sample D than for comparable samples on 3C-SiC. Both these findings can be interpreted as more efficient DP relaxation, which then starts to dominate spin relaxation already at lower temperatures and additionally leads to shorter spin-relaxation times. The strength of DP relaxation can be estimated for sample D as its room-temperature mobility $\mu_e^D = 75$ cm^2/Vs has been determined by Hall measurements [51]. Our simulations reproduce μ_e^D for a dislocation density of $n_{disl} = 4 \times 10^{10}$ cm^{-2}, allowing us to further simulate the corresponding weighted momentum scattering time $(Q\tau_p)_{total}$ according to Eq. (9) and to estimate the spin-splitting constant $\gamma_e = 6$ eVÅ^3 via Eqs. (7) and (8). Such a high value for the spin-splitting constant indicates an important role of dislocations for spin relaxation, which can, however, only be clarified by a more thorough experimental and theoretical study.

V. SUMMARY

Summarizing, we have experimentally investigated the electron spin dynamics in cubic GaN for temperatures from 15 K up to 500 K, magnetic fields up to 1 T and doping densities from 6×10^{16} cm^{-3} up to 1.5×10^{19} cm^{-3}. We observe a nonmonotonic temperature dependence and a characteristic flattening of the magnetic field dependence of spin relaxation for increasing temperature at moderate doping levels. In contrast, the spin-relaxation time is independent of temperature and magnetic field strength at degenerate doping levels. In addition, spin relaxation shows a nonmonotonic doping density dependence. All these findings are consistently explained by the dominance of spin relaxation of localized electrons up to moderate temperatures and doping levels, with a transition to Dyakonov-Perel dominated spin relaxation for higher temperatures and doping densities. Quantitative agreement to predictions of Dyakonov-Perel theory requires the assumption of a larger spin-splitting constant than theoretically predicted. Possible sources for large effective spin splittings have been discussed, including charged dislocations and a phase mixture with hexagonal GaN.

ACKNOWLEDGMENTS

[1] M. W. Wu, J. H. Jiang, and M. Q. Weng, Phys. Rep. **493**, 61 (2010).

[2] J. H. Jiang and M. W. Wu, Phys. Rev. B **79**, 125206 (2009).

[3] M. I. Dyakonov and V. I. Perel, Sov. Phys. Solid State **13**, 3023 (1972).

[4] D. J. Chadi, Phys. Rev. B **16**, 790 (1977).

[5] R. Winkler, in *Spin-Orbit Coupling Effects in Two-Dimensional Electron and Hole Systems*, edited by D. D. Awschalom and N. Samarth (Springer-Verlag, Berlin, 2003).

[6] *Semiconductor Spintronics and Quantum Computation*, edited by D. D. Awschalom and N. Samarth (Springer-Verlag, Berlin, 2002).

[7] *Spin Physics in Semiconductors*, edited by M. I. Dyakonov (Springer-Verlag, Berlin, 2008).

[8] I. Zutic, J. Fabian, and S. D. Sarma, Rev. Mod. Phys. **76**, 323 (2004).

[9] J. Rudolph, D. Hägele, H. M. Gibbs, G. Khitrova, and M. Oestreich, Appl. Phys. Lett. **82**, 4516 (2003); M. Oestreich, J. Rudolph, R. Winkler, and D. Hägele, Superlattices Microstruct. **37**, 306 (2005).

[10] J. H. Buß, J. Rudolph, F. Natali, F. Semond, and D. Hägele, Appl. Phys. Lett. **95**, 192107 (2009).

[11] J. H. Buß, J. Rudolph, F. Natali, F. Semond, and D. Hägele, Phys. Rev. B **81**, 155216 (2010).

[12] J. H. Buß, J. Rudolph, S. Starosielec, A. Schaefer, F. Semond, Y. Cordier, A. D. Wieck, and D. Hägele, Phys. Rev. B **84**, 153202 (2011).

[13] J. H. Buß, J. Rudolph, S. Shvarkov, H. Hardtdegen, A. D. Wieck, and D. Hägele, Appl. Phys. Lett. **102**, 192102 (2013).

[14] J. H. Buß, J. Rudolph, S. Shvarkov, F. Semond, D. Reuter, A. D. Wieck, and D. Hägele, Appl. Phys. Lett. **103**, 092401 (2013).

[15] J. Rudolph, J. H. Buß, and D. Hägele, Phys. Status Solidi B **251**, 1850 (2014).

[16] S. Krishnamurthy, M. van Schilfgaarde, and N. Newman, Appl. Phys. Lett. **83**, 1761 (2003).

[17] Z. G. Yu, S. Krishnamurthy, M. van Schilfgaarde, and N. Newman, Phys. Rev. B **71**, 245312 (2005).

[18] J. H. Buß, A. Schaefer, T. Schupp, D. J. As, D. Hägele, and J. Rudolph, Appl. Phys. Lett. **105**, 182404 (2014).

[19] J. H. Buß, J. Rudolph, T. Schupp, D. J. As, K. Lischka, and D. Hägele, Appl. Phys. Lett. **97**, 062101 (2010).

[20] S. Döhrmann, D. Hägele, J. Rudolph, M. Bichler, D. Schuh, and M. Oestreich, Phys. Rev. Lett. **93**, 147405 (2004).

[21] G. Dresselhaus, Phys. Rev. **100**, 580 (1955).

[22] G. E. Pikus, V. A. Marushchak, and A. N. Titkov, Sov. Phys. Semicond. **22**, 115 (1988).

[23] M. I. Dyakonov, V. A. Marushchak, V. I. Perel, and A. N. Titkov, Sov. Phys. JETP **63**, 655 (1986).

[24] D. Hägele, S. Döhrmann, J. Rudolph, and M. Oestreich, Adv. Solid State Phys. **45**, 253 (2005).

[25] *Optical Orientation*, edited by F. Meier and B. P. Zakharchenya (North-Holland, Amsterdam, 1984).

[26] J. Fabian, A. Matos-Abiaguea, C. Ertlera, P. Stano, and I. Zutic, Acta Phys. Slovaca **57**, 565 (2007).

[27] S. Oertel, J. Hübner, and M. Oestreich, Appl. Phys. Lett. **93**, 132112 (2008).

[28] D. Jena, Phys. Rev. B **70**, 245203 (2004).

[29] We consider only nonquantizing magnetic fields here, where Landau level quantization does not dominate.

[30] M. I. Dyakonov and V. I. Perel, Sov. Phys. JETP **38**, 177 (1974).

[31] E. L. Ivchenko, Sov. Phys. Solid State **15**, 1048 (1973).

[32] J. Y. Fu and M. W. Wu, J. Appl. Phys. **104**, 093712 (2008).

[33] K. Shen, J. Fu, and M. Wu, Solid State Commun. **151**, 1924 (2011).

[34] K. V. Kavokin, Semicond. Sci. Technol. **23**, 114009 (2008).

[35] I. A. Merkulov, A. L. Efros, and M. Rosen, Phys. Rev. B **65**, 205309 (2002).

[36] M. Syperek, D. R. Yakovlev, I. A. Yugova, J. Misiewicz, I. V. Sedova, S. V. Sorokin, A. A. Toropov, S. V. Ivanov, and M. Bayer, Phys. Rev. B **84**, 085304 (2011).

[37] A. Greilich, A. Pawlis, F. Liu, O. A. Yugov, D. R. Yakovlev, K. Lischka, Y. Yamamoto, and M. Bayer, Phys. Rev. B **85**, 121303 (2012).

[38] K. V. Kavokin, Phys. Rev. B **64**, 075305 (2001).

[39] R. I. Dzhioev, K. V. Kavokin, V. L. Korenev, M. V. Lazarev, B. Y. Meltser, M. N. Stepanova, B. P. Zakharchenya, D. Gammon, and D. S. Katzer, Phys. Rev. B **66**, 245204 (2002).

[40] Z. Chen, S. G. Carter, R. Bratschitsch, P. Dawson, and S. T. Cundiff, Nat. Phys. **3**, 265 (2007).

[41] R. J. Elliott, Phys. Rev. **96**, 266 (1954).

[42] Y. Yafet, Solid State Phys. **14**, 1 (1963).

[43] P. H. Song and K. W. Kim, Phys. Rev. B **66**, 035207 (2002).

[44] G. L. Bir, A. G. Aronov, and G. E. Pikus, Sov. Phys. JETP **42**, 705 (1976).

[45] A. D. Margulis and V. A. Margulis, Sov. Phys. Solid State **25**, 918 (1983).

[46] F. X. Bronold, I. Martin, A. Saxena, and D. L. Smith, Phys. Rev. B **66**, 233206 (2002).

[47] D. Paget, Phys. Rev. B **24**, 3776 (1981).

[48] W. O. Putikka and R. Joynt, Phys. Rev. B **70**, 113201 (2004).

[49] D. J. As, in *III-Nitride Semiconductor Materials: Growth*, edited by M. O. Manasreh and I. T. Ferguson (Taylor and Francis, New York, 2003), Chap. 9.

[50] D. J. As, S. Potthast, J. Schörmann, S. F. Li, K. Lischka, H. Nagasawa, and M. Abe, Mater. Sci. Forum **527-529**, 1489 (2006).

[51] O. Brandt, in *Group III Nitride Semiconductor Compounds*, edited by B. Gil (Clarendon Press, Oxford, 1998).

[52] T. Schupp, K. Lischka, and D. J. As, J. Cryst. Growth **312**, 1500 (2010).

[53] The doping densities n_D are inferred from a standard curve calibrated via secondary ion mass spectrometry and C-V measurements.

[54] D. J. As, T. Frey, D. Schikora, K. Lischka, V. Cimalla, J. Pezoldt, R. Goldhahn, S. Kaiser, and W. Gebhardt, Appl. Phys. Lett. **76**, 1686 (2000).

[55] D. J. As, F. Schmilgus, C. Wang, B. Schöttker, D. Schikora, and K. Lischka, Appl. Phys. Lett. **70**, 1311 (1997).

[56] J. Holst, L. Eckey, A. Hoffmann, I. Broser, B. Schöttker, D. J. As, D. Schikora, and K. Lischka, Appl. Phys. Lett. **72**, 1439 (1998).

[57] D. J. As, Proc. SPIE **7608**, 76080G (2010).

[58] The oscillatory structures on the PL spectra are due to Fabry-Perot interferences.

[59] J. De-Sheng, Y. Makita, K. Ploog, and H. J. Queisser, J. Appl. Phys. **53**, 999 (1982).

[60] M. W. Bayerl, M. S. Brandt, T. Graf, O. Ambacher, J. A. Majewski, M. Stutzmann, D. J. As, and K. Lischka, Phys. Rev. B **63**, 165204 (2001).

[61] J. H. Buß, T. Schupp, D. J. As, D. Hägele, and J. Rudolph, J. Appl. Phys. **118**, 225701 (2015).

[62] G. Wang, C. R. Zhu, B. L. Liu, H. Ye, A. Balocchi, T. Amand, B. Urbaszek, H. Yang, and X. Marie, Phys. Rev. B **90**, 121202 (2014).

[63] B. Urbaszek, X. Marie, T. Amand, O. Krebs, P. Voisin, P. Maletinsky, A. Högele, and A. Imamoglu, Rev. Mod. Phys. **85**, 79 (2013).

[64] We note that the approach of Ref. [12] with an experimental determination of the momentum scattering time for the wurtzite phase of GaN is useful as the efficiency factors reduce to $\gamma_1 = 1$ in this case due to the dominance of the linear-in-k Rashba term.

[65] B. Pödör, Phys. Status Solidi B **16**, K167 (1966).

[66] H. M. Ng, D. Doppalapudi, T. D. Moustakas, N. G. Weimann, and L. F. Eastman, Appl. Phys. Lett. **73**, 821 (1998).

[67] D. J. As, D. Schikora, A. Greiner, M. Lübbers, J. Mimkes, and K. Lischka, Phys. Rev. B **54**, R11118(R) (1996).

[68] R. L. Petritz and W. W. Scanlon, Phys. Rev. **97**, 1620 (1955).

[69] J. Bardeen and W. Shockley, Phys. Rev. **80**, 72 (1950).

[70] J. D. Zook, Phys. Rev. **136**, A869 (1964).

[71] D. Chattopadhyay and H. J. Queisser, Rev. Mod. Phys. **53**, 745 (1981).

[72] A. M. Kreshchuk, S. V. Novikov, I. G. Savel'ev, T. A. Polyanskaya, B. Pödör, G. Reményi, and G. Kovács, Acta Phys. Pol. A **94**, 415 (1996).

[73] D. J. As and K. Lischka, in *Nonpolar Cubic III-Nitrides: From the Basics of Growth to Device Applications*, edited by M. Henini (Elsevier, Oxford, 2013).

[74] G. Ramírez-Flores, H. Navarro-Contreras, A. Lastras-Martínez, R. C. Powell, and J. E. Greene, Phys. Rev. B **50**, 8433 (1994).

[75] S. K. Pugh, D. J. Dugdale, S. Brand, and R. A. Abram, Semicond. Sci. Technol. **14**, 23 (1999).

[76] H. Siegle, L. Eckey, A. Hoffmann, C. Thomsen, B. K. Meyer, D. Schikora, M. Hankeln, and K. Lischka, Solid State Commun. **96**, 943 (1995).

[77] T. Lei, M. Fanciulli, R. J. Molnar, T. D. Moustakas, R. J. Graham, and J. Scanlon, Appl. Phys. Lett. **59**, 944 (1991).

[78] K. Kim, W. R. L. Lambrecht, and B. Segall, Phys. Rev. B **53**, 16310 (1996).

[79] S.-H. Park and S.-L. Chuang, J. Appl. Phys. **87**, 353 (2000).

[80] K. Shimada, T. Sota, and K. Suzuki, J. Appl. Phys. **84**, 4951 (1998).

[81] M. Kohno, T. Nakamura, T. Kataoka, R. Katayama, and K. Onabe, Phys. Status Solidi C **5**, 1805 (2008); J. N. Kuznia, J. W. Yang, Q. C. Chen, S. Krishnankutty, M. A. Khan, T. George, and J. Frietas, Appl. Phys. Lett. **65**, 2407 (1994); H. Okumura, S. Misawa, T. Okahisa, and S. Yoshida, J. Cryst. Growth **136**, 361 (1994); S. V. Novikov, N. M. Stanton, R. P. Campion, R. D. Morris, H. L. Geen, C. T. Foxon, and A. J. Kent, Semicond. Sci. Technol. **23**, 015018 (2008).

[82] The experimental values of the spin-relaxation time for $T > 300$ K were taken from Ref. [18].

[83] J. J. Krich and B. I. Halperin, Phys. Rev. Lett. **98**, 226802 (2007).

[84] R. M. Kemper, T. Schupp, M. Häberlen, T. Niendorf, H.-J. Maier, A. Dempewolf, F. Bertram, J. Christen, R. Kirste, A. Hoffmann, J. Lindner, and D. J. As, J. Appl. Phys. **110**, 123512 (2011).

[85] J. A. Majewski and P. Vogel, MRS Internet J. N. S. R. **3**, 21 (1998).

[86] V. I. Melnikov and E. I. Rashba, Sov. Phys. JETP **34**, 1353 (1972).

[87] A. T. Blumenau, J. Elsner, R. Jones, M. I. Heggie, S. Öberg, T. Frauenheim, and P. R. Briddon, J. Phys.: Condens. Matter **12**, 10223 (2000).

[88] A. Bhattacharya, M. Z. Baten, and P. Bhattacharya, Appl. Phys. Lett. **108**, 042406 (2016).

[89] A. Schaefer, J. H. Buß, T. Schupp, A. Zado, D. J. As, D. Hägele, and J. Rudolph, J. Appl. Phys. **117**, 093906 (2015).

[90] M. Y. Petrov, I. V. Ignatiev, S. V. Poltavtsev, A. Greilich, A. Bauschulte, D. R. Yakovlev, and M. Bayer, Phys. Rev. B **78**, 045315 (2008).

[91] J. H. Jiang, Y. Y. Wang, and M. W. Wu, Phys. Rev. B **77**, 035323 (2008).

[92] N. N. Zinov'ev, A. V. Andrianov, B. Y. Averbukh, I. D. Yaroshetskii, S. T. Cheng, L. C. Jenkins, S. E. Hooper, C. T. Foxon, and J. W. Orton, Semicond. Sci. Technol. **10**, 1117 (1995).

[93] C. Herring and M. Flicker, Phys. Rev. **134**, A362 (1964).